CERN-SND@LHC-NOTE-2024-001
February 14, 2024

Analytical Tools for the Evaluation of the AvdSND FAR Magnetic Spectrometer Performance

V. Scalera[1,2]

Abstract

The Advanced SND project is an extension of the SND@LHC experiment, a compact standalone experiment designed to perform measurements with high-energy neutrinos in range 100 GeV–1 TeV produced at the LHC. A possible extension consists in the introduction of a new magnetic spectrometer (denoted as FAR detector) in the region $7.2 < \eta < 8.4$ meant to operate during LHC run 4. This note presents a performance analysis of the new detector's spectrometer, by mean of analytical and semianalytical tools, well behaved for joint optimization in further electromagnetic design phase. The model presented is validated via Montecarlo simulations using GEANT4, and the momentum resolution is evaluated analytically as a function of the detector geometry and magnetic field strength.

[1] *Sezione INFN di Napoli, Napoli, 80126, Italy*
[2] *Università di Napoli Parthenope, Napoli, 80143, Italy*

VERSION	DATE	COMMENTS
01	14.02.2024	First version

Contents

1 Introduction

Spectrometers are fundamental components of particle detector used to measure the particles momentum and charge. Using strong magnetic fields particle trajectory is deflected, particular devices (hereafter called tracking stations or trackers) detect the particle's position when hit, and momentum is estimated using the reconstructed trajectory.
The design optimization often involves the coupling of a physical and an engineering analysis. The physical design defines the momentum resolution, giving the length of the magnets, the magnetic fields and the position of the trackers, the engineering design defines the power consumption and the construction cost, giving the coil thickness, the iron yoke thickness and the magneto-motive force as main output parameters.
Both analysis rely on numerical tools such as Monte Carlo simulation to evaluate the momentum resolution and FEM or BEM analysis to evaluate the magneto-static field, the temperature and the mechanical stress in the magnet.
However, numerical techniques do not allow to couple the two analysis, and optimization processes are generally very time consuming. Analytical models play an important role both for a coupled analysis involving physical and engineering requirements at the same time and for the optimization procedure.
This work proposes a mathematical framework for the geometrical design of a spectrometer based on analytical and semi-analytical models.
The study case concern the AdvSND experiment [1], an extension of the already operative SND@LHC experiment, which includes two detectors located in two different positions along the LHC accelerator covering two complementary angular regions: the FAR and NEAR detectors. The analysis reported applies to the new proposed spectrometer magnet of the FAR detector which is, in particular, operating in the pseudorapidity region $7.2 < \eta < 8.4$.
Due to the limited available space, the calorimeter of the FAR detector is magnetized and it is used as part of the spectrometer, as shown in Figure 1, in order to reduce the total length. The tracking station are placed at the end of the calorimeter and around the magnet (tracking stations 2, 3 and 4 in Figure), and high precision trackers are located inside the target are used to detect the position where the particle is created.

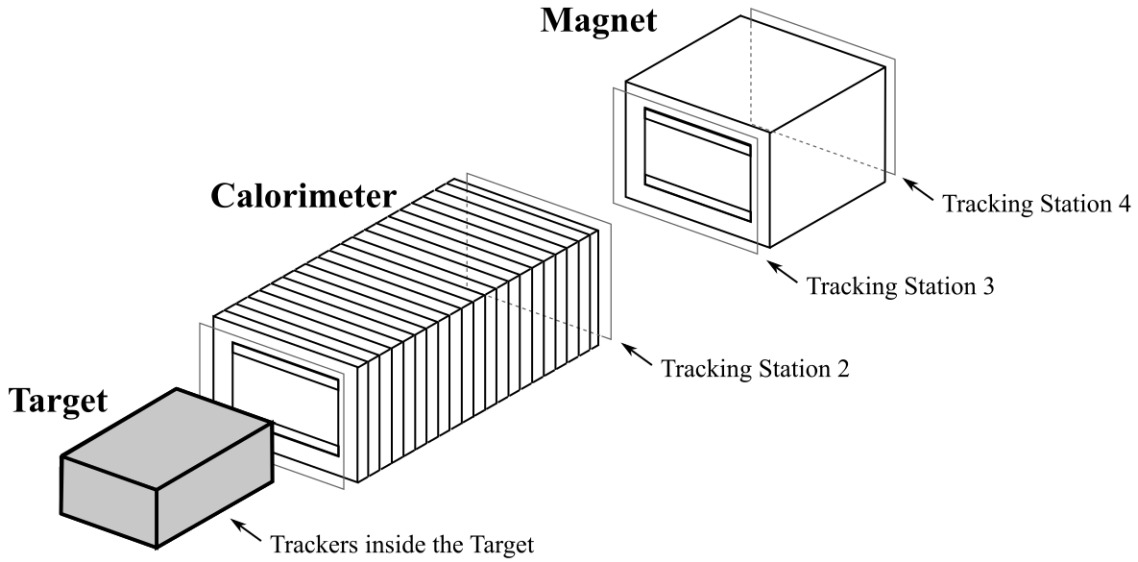

Figure 1: Scheme of the AdvSND FAR detector.

2 Mathematical Model

Every particle flight is characterized by a set of random variables and it can be modeled as an event of a sample space. In particular, we have

$$\Omega \to \left\{ \underbrace{P, X_0, S_0, \Theta_0,}_{\text{Particle Initial State}} \quad \underbrace{\Delta_1, \Delta_2, \Delta_3, \Delta_4,}_{\text{Measurement Errors}} \quad \underbrace{\Theta_{\sigma 01},\, S_{\sigma 01},\, \Theta_{\sigma 12},\, S_{\sigma 12},\, \Theta_{\sigma 34},\, S_{\sigma 34}}_{\text{Scattering Effects}} \right\} \quad (1)$$

where P is the particle momentum, S_0, X_0 and Θ_0 are the initial position and angle of the particle, Δ is the set of measurement error on the tracking stations, and Θ_σ and S_σ are the deviations and displacements due to the scattering in solids.
Consider the notation in Figure 2: the target, the calorimeter and the magnet are represented by the rectangles, the tracking stations are placed on both side of each magnet, and in the target (rectangle on the left). At each tracking station the state of the particle is defined by the angle Θ_i and the vertical displacement S_i (as shown in the Figure 2 on the right), the vertical displacement is measured by the tracker, while the angle is not directly measurable.
The particle dynamic is modeled using classical equation of motion in the small angle approximation. Given the particle momentum $P = p$, the equations of motion are

$$\text{Displacement:} \begin{cases} S_4 - S_3 = \Theta_3\, x_{34} + \dfrac{qB_2}{2p} x_{34}^2 + S_{\sigma 34} \\ S_3 - S_2 = \Theta_2\, x_{23} \\ S_2 - S_1 = \Theta_1 x_{12} + \dfrac{qB_1^*}{2p} x_{12}^2 + S_{\sigma 12} \\ S_1 - S_0 = \Theta_0 x_{01} + S_{\sigma 01} \end{cases} \quad (2)$$

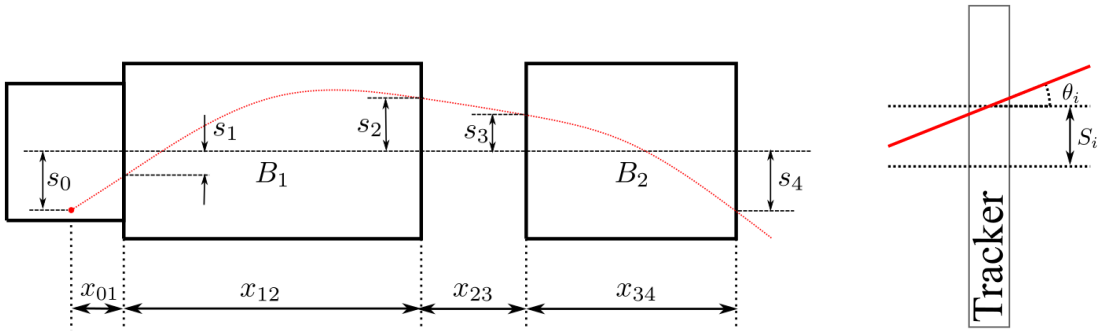

Figure 2: Notation used for the geometrical quantities (lengths and angles). The first rectangle from the left is the target, the second is the calorimeter and the third is the magnet. The red curve is the particle trajectory, x_i are used to denote the lengths along the detector axis and s_i are used to denote the displacement from the axis. On the right, is represented the angle θ between the particle trajectory and the tracker plane.

$$\text{Angle:} \begin{cases} \Theta_3 = \Theta_2 \\ \Theta_2 = \Theta_1 + \dfrac{qB_1^*}{p} x_{12} + \Theta_{\sigma 12} \\ \Theta_1 = \Theta_0 + \Theta_{\sigma 01} \end{cases} \tag{3}$$

where the superscript $*$ denote a corrected field to take into account the presence of air gaps in the calorimeter, and the quantities with subscript σ are the effects of the scattering and they are random variables.
Replacing the angle equations (3) in the displacement equations (2) it yields

$$\begin{aligned} S_{43} &= S_4 - S_3 = \Theta_0\, x_{34} + \frac{qB_1^*}{p} x_{12} x_{34} + \Theta_{\sigma 01} x_{34} + \Theta_{\sigma 12}\ x_{34} + \frac{qB_2}{2p} x_{34}^2 + S_{\sigma 34} \\ S_{32} &= S_3 - S_2 = \Theta_0\, x_{23} + \frac{qB_1^*}{p} x_{12} x_{23} + \Theta_{\sigma 01} x_{23} + \Theta_{\sigma 12}\ x_{23} \\ S_{20} &= S_2 - S_0 = \Theta_0\, (x_{12} + x_{01}) + \frac{qB_1^*}{2p} x_{12}^2 + \Theta_{\sigma 01} x_{12} + S_{\sigma 12} + S_{\sigma 01} \end{aligned} \tag{4}$$

2.1 Momentum Estimator

For the sake of simplicity, we look for a momentum estimator using a linear combination of the measured particle displacements. Using the difference of displacement given in (4) we have

$$\alpha S_{43} + \beta S_{32} + \gamma S_{20} = \ (\Theta_0 + \Theta_{\sigma 01})(\alpha x_{34} + \beta x_{23} + \gamma x_{02}) + \frac{q}{2p} \mathcal{B}(\alpha, \beta, \gamma) + \Sigma(\alpha, \beta, \gamma) \tag{5}$$

where α, β and γ are coefficients to be chosen and $x_{02} = x_{01} + x_{12}$, and Σ and $\mathcal{B}$ are the effects of scattering and magnetic field respectively

$$\mathcal{B}(\alpha,\beta,\gamma) = (2\alpha x_{34} + 2\beta x_{23} + \gamma x_{12})B_1^* x_{12} + \alpha B_2 x_{34}^2 \tag{6}$$
$$\Sigma(\alpha,\beta,\gamma) = (\alpha x_{34} + \beta x_{23})\,\Theta_{\sigma 12} + \gamma S_{\sigma 12} + \gamma(S_{\sigma 01} - x_{01}\Theta_{\sigma 01}) + \alpha S_{\sigma 34} \tag{7}$$

Note that Σ and $\mathcal{B}$ also depend on the spacing between tracking stations x_{ij} although it is not explicitly written in notation (6) and (7). Moreover, Σ is a random variable. In order to remove the dependence of the momentum on the unknown initial angle Θ_0, the coefficients α, β and γ must satisfy the constraint

$$\alpha x_{34} + \beta x_{23} + \gamma x_{02} = 0 \tag{8}$$

so that (6) and (7) are recast as functions of α and γ only

$$\mathcal{B}(\alpha,\gamma) = \alpha B_2 x_{34}^2 - \gamma B_1^* x_{12}(x_{12} + 2x_{01}) \tag{9}$$
$$\Sigma(\alpha,\gamma) = \alpha S_{\sigma 34} + \gamma(S_{\sigma 12} - x_{02}\Theta_{\sigma 12}) + \gamma(S_{\sigma 01} - x_{01}\Theta_{\sigma 01}) \tag{10}$$

and the reciprocal of the momentum is given by

$$\frac{1}{p} = \frac{2}{q}\frac{\alpha S_{43} + \beta S_{32} + \gamma S_{20} - \Sigma(\alpha,\gamma)}{\mathcal{B}(\alpha,\gamma)} \tag{11}$$

The tracking station measurement is affected by error, modeled by defining the measured displacement $\overline{S}_i = S_i + \Delta_i$, where Δ_i is a random variable with zero mean and standard deviation ε.
Using the displacements available from measurements (affected by error), we define the estimator

$$\hat{\Pi}(\alpha,\gamma) = \frac{2}{q}\frac{\alpha\ \overline{S}_4 + (\beta-\alpha)\ \overline{S}_3 + (\gamma-\beta)\ \overline{S}_2 - \gamma\ \overline{S}_0}{\mathcal{B}(\alpha,\gamma)} \tag{12}$$

since the scattering error has zero average, the expected value of the estimator (12) yields the reciprocal of the momentum

$$\mathbb{E}\left[\ \hat{\Pi}\ \middle|\ P = p\ \right] = \frac{1}{p} \tag{13}$$

where the operator $\mathbb{E}$ is the expected value and the random variables after the | sign are given (conditioned probability).

2.2 Standard Deviation and Distortion

In order to evaluate the error, an estimate of the momentum standard deviation is required. After some algebra, (12) and (11) give

$$\sigma\left[\hat{\Pi}|P = p\right] = \frac{2}{q}\ \frac{\sqrt{\varepsilon^2[\alpha^2 + (\beta-\alpha)^2 + (\gamma-\beta)^2 + \gamma^2] + \sigma_\Sigma^2(\alpha,\gamma)}}{|\mathcal{B}(\alpha,\gamma)|} \tag{14}$$

where σ is the standard deviation, and σ^2_Σ is the variance due to scattering (derived in the appendix)

$$\sigma^2_\Sigma(\alpha,\gamma) = \frac{P_0^2}{p^2}\left[\frac{\gamma^2}{3}\left(\frac{x_{01}^3}{X_\mathrm{W}} + \frac{x_{12}^3 + 3x_{01}x_{12}x_{02}}{X^*_\mathrm{Fe}}\right) + \frac{\alpha^2}{3}\frac{x_{34}^3}{X_\mathrm{Fe}}\right] \tag{15}$$

with P_0 is an empirical constant, and X_Fe and X_W are the radiation length of the iron and tungsten respectively, the asterisk $*$ denotes that the radiation length must include a correction to take into account the fact that the spectrometer has air gaps between the iron slabs.
The momentum resolution (or momentum uncertainty) is defined as $\sigma[\hat{P}|P=p\,]/p$. in the following the condition $P = p$ is omitted to keep the notation simple. Assuming the standard deviation to be much smaller than the mean of $\hat{\Pi}$, the resolution on the momentum is obtained using the propagation of uncertainty, i.e. truncating the Taylor expansion of $\hat{P} = \hat{\Pi}^{-1}$ at the first order around the expected value. The resolution on the momentum is then approximated with the resolution on its reciprocal

$$\sigma\left[\hat{P}\right] \approx \sqrt{\left(\frac{\mathrm{d}}{\mathrm{d}\hat{\Pi}}\hat{P}\right)^2}\Bigg|_{\hat{\Pi}=\mathbb{E}[\hat{\Pi}]} \sigma[\hat{\Pi}] = p^2\,\sigma[\hat{\Pi}] \implies \frac{\sigma[\hat{P}]}{p} \approx p\cdot\sigma[\hat{\Pi}] \tag{16}$$

This approximation usually holds for small values of the standard deviation, roughly up to $\sigma[\hat{P}]/p \approx 0.15$, but it predicts better resolution than the real ones, especially for higher values of $\sigma[\hat{P}]/p$.
Higher order approximations provide better analytical results, however the analytical formulation quickly become complex while the improvement is modest.
A better approach to evaluate $\sigma[\hat{P}]$ require the use of numerical integration. By definition, the standard deviation of the momentum is given by

$$\sigma[\hat{P}] = \int_{-\infty}^{+\infty}\left(\left|\frac{1}{x}\right| - \overline{P}\right)^2 f_{\hat{\Pi}}(x)\,\mathrm{d}x \qquad \text{with} \qquad \overline{P} = \int_{-\infty}^{+\infty}\left|\frac{1}{x}\right| f_{\hat{\Pi}}(x)\,\mathrm{d}x \tag{17}$$

where $f_{\hat{\Pi}}$ is the probability density function of the random variable $\hat{\Pi}$.
Although $f_{\hat{\Pi}}$ is not known exactly, it is reasonable to assume a Gaussian distribution whose mean and standard deviation are given by formulas (13) and (14), namely

$$f_{\hat{\Pi}}(x) = C\exp\left(-\frac{(x-\mu_{\hat{\Pi}})^2}{2\sigma^2_{\hat{\Pi}}}\right) \tag{18}$$

where $\mu_{\hat{\Pi}} = \mathbb{E}\left[\hat{P}\right] = p^{-1}$, $\sigma_{\hat{\Pi}} = \sigma[\hat{\Pi}]$ is given by (14) and C is a constant such that

$$\int_{1/p_\mathrm{max}}^{+\infty} f_{\hat{\Pi}}(x)\,\mathrm{d}x = 1 \tag{19}$$

Such assumption is exact if the trackers errors Δ_i have Gaussian distribution, since the scattering displacements are Gaussians and the sum of Gaussian distributions

have a Gaussian distribution itself.
Note that $\overline{P}$ in (17) has a non integrable singularity (and σ_P is undefined as well). This problem is solved by imposing a cut-off value for the particle momentum $p_{\max}$, and excluding from the sample all the measurement above this threshold. The threshold value is chosen based on the maximum momentum expected for the produced particles, momentum above $p_{\max}$ are considered as measurement errors and are not included in the statistics. Equation (17) is recast as

$$\sigma\left[\hat{P}\right]^2 = \int_{1/p_{\max}}^{+\infty} \left(\left|\frac{1}{x}\right| - \overline{P}\right)^2 f_{\hat{1\!\!1}}(x)\ \mathrm{d}x \qquad \text{with} \qquad \overline{P} = \int_{1/p_{\max}}^{+\infty} \left|\frac{1}{x}\right| f_{\hat{1\!\!1}}(x)\ \mathrm{d}x \tag{20}$$

which is well-defined and integrable numerically. Remarkably, the singularity in the expected momentum exists also when the uncertainty is small, however, the probability of having samples close to the singularity is so small that they hardly appear unless the statistical sample size is extremely high. This also implies that the threshold $\sigma[\hat{P}]/p \approx 0.15$ may actually be smaller if the statistical sample size is large enough and no cut-off is applied.
Equation (20) can be recast in an adimentional form as

$$\frac{\sigma^2\left[\hat{P}\right]}{p^2} = \int_{T}^{+\infty} \left(\left|\frac{1}{x}\right| - \frac{\overline{P}}{p}\right)^2 f(x)\ \mathrm{d}x \qquad \text{with} \qquad \frac{\overline{P}}{p} = \int_{T}^{+\infty} \left|\frac{1}{x}\right| f(x)\ \mathrm{d}x \tag{21}$$

where

$$f(x) = \frac{\exp\left(-\dfrac{(x-1)^2}{2R^2}\right)}{\displaystyle\int_{T}^{+\infty} \exp\left(-\frac{(y-1)^2}{2R^2}\right)\ \mathrm{d}y} \tag{22}$$

and $R = \sigma_{\hat{1\!\!1}}/\mu_{\hat{1\!\!1}}$ is the resolution of the momentum reciprocal and $T = p/p_{\max}$ is the ratio with the threshold momentum. Figure 3 and Figure 4 show $\sigma_{\hat{P}}/p$ and $(\overline{P} - p)/p$ as function of R for several values of $p/p_{\max}$. Two fundamental results are visible from the plots and need special attentions:

- The momentum estimator is distorted, i.e. its expected value does not coincide with the expected value of quantity to be estimated
- The first order approximation (16) results in a optimistic prediction for the resolution, compared with the real spectrometer performance

The estimator distortion can be readily proved by mean of the Jensen's inequality

$$\varphi \text{ is convex} \implies \varphi(\mathbb{E}[X]) \leq \mathbb{E}[\varphi(X)]$$

In order to have a quantitative result, the expected value of $\hat{P}$ is recast as

$$\mathbb{E}\left[\hat{P}|P = p\right] = p\ \mathbb{E}\left[\frac{1}{1 + \mathcal{E}(\alpha, \beta, \gamma)}\right] \tag{23}$$

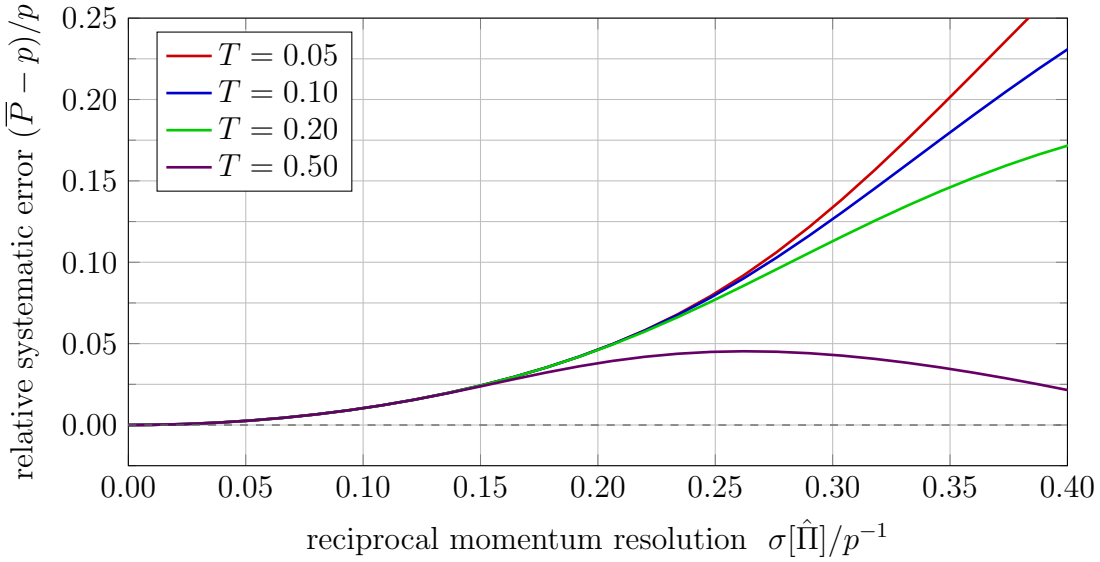

Figure 3: Average value of the relative error as function of the resolution of $1/p$ for different values of the threshold $p_{\max}$.

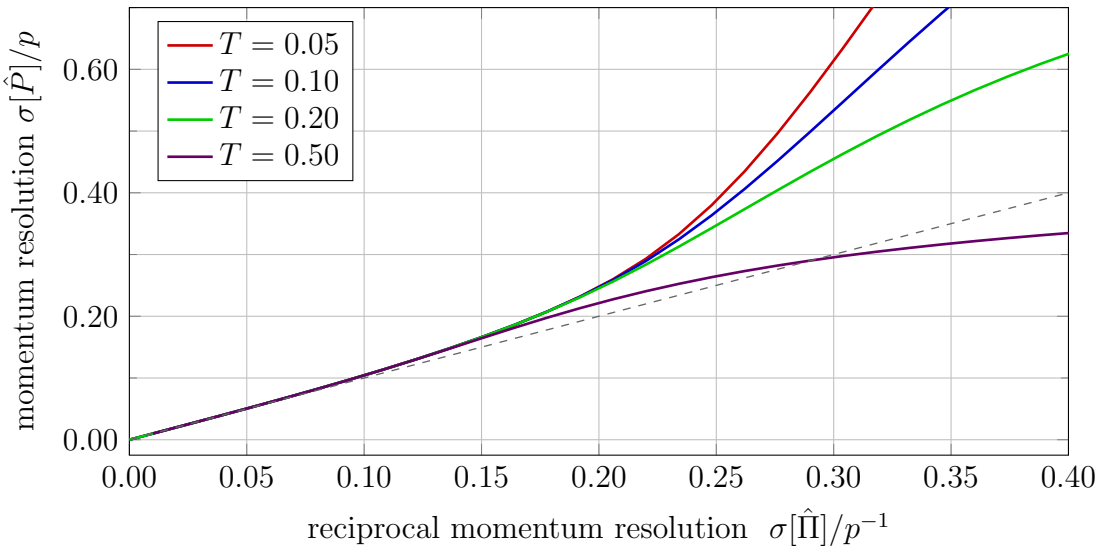

Figure 4: Standard deviation of the relative error as function of the resolution of $1/p$ for different values of the threshold $p_{\max}$. The gray dashed line represents the identity function, i.e. the resolution predicted by the first order model.

where we used the fact that the scattering effects Σ and tracking errors Δ_i are independent, and the random variable $\mathcal{E}(\alpha, \beta, \gamma)$ is

$$\mathcal{E}(\alpha, \beta, \gamma) = \frac{\alpha\Delta_4 + (\beta - \alpha)\Delta_3 + (\gamma - \beta)\Delta_2 + \gamma\Delta_0}{\alpha S_{43} + \beta S_{32} + \gamma S_{20}} \tag{24}$$

and Δ_i is the measurement error at the i-th tracking station.
If we consider a momentum p much smaller than the cut-off threshold $p_{\max}$, we

can assume that $\mathcal{E}$ is symmetric, namely $\mathbb{E}[\mathcal{E}^{2n+1}] = 0$ for every natural number n. Expanding the random variable in (23) in the variable $\mathcal{E}$, it yields

$$\mathbb{E}\left[\frac{1}{1+\mathcal{E}(\alpha,\beta,\gamma)}\right] = \mathbb{E}\left[1+\sum_{n=1}^{\infty}(-1)^n\mathcal{E}^n\right] = 1+\sum_{n=1}^{\infty}\mathbb{E}\left[\mathcal{E}^{2n}\right] > 1 \qquad (25)$$

The last equation proves that the estimator is distorted, the distortion depends on the momentum and on the tracking error, and for small $\mathcal{E}$, the systematic error has a quadratic dependence on $\sigma[\hat{\Pi}]/p^{-1}$ if the scattering is negligible. For higher values of p the cut-off mechanism comes into play and the systematic error decrease until eventually becomes negative (see Figure 3).
Concerning the resolution, Figure 5 shows an example of comparison between (16) and (20) for $p_{\max} = 2000$ GeV/c and $p_{\max} = 3000$ GeV/c. As anticipated, the linear approximation prediction may result in a wrong design of the spectrometer, which will not achieve the desired resolution. This discrepancy can be reduced with a proper choice of the cut-off threshold $p_{\max}$. According to the curves in Figures 3 and 4, $T = 0.5$ is reasonably close to the linear approximation with a relatively small systematic error. If, for example, the maximum momentum expected is 1000 GeV/c, a convenient value for $p_{\max}$ should not exceed 2000 GeV/c.

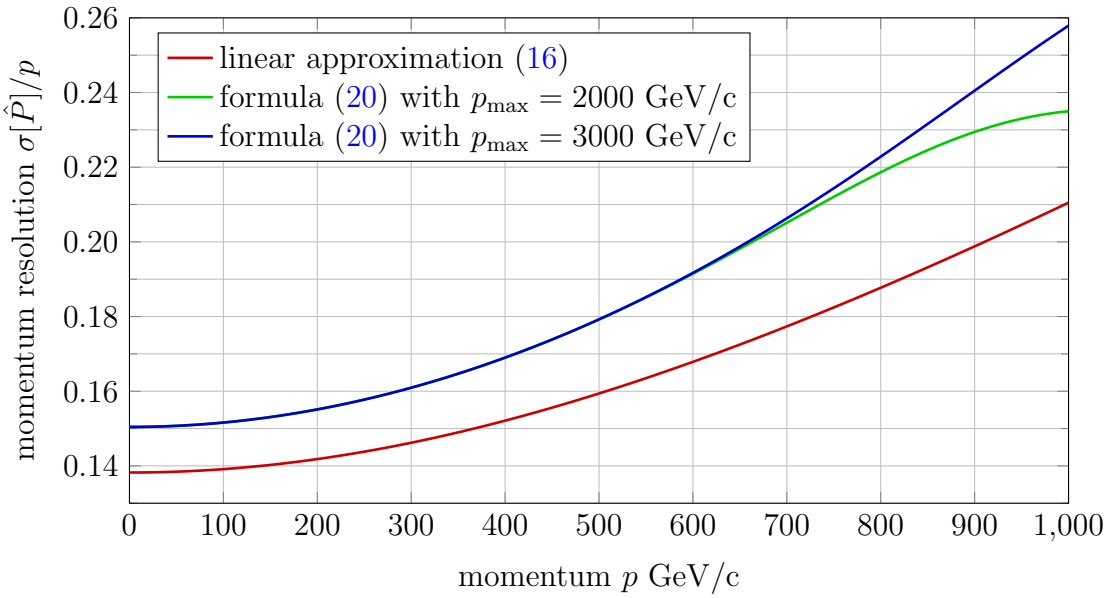

Figure 5: Comparison between the first order approximation (16) and the semianalytical equation (20) for two different values of the cut-off threshold.

3 Design of the AdvSND Detector

Equations (14) and (21) can be used as design tool for spectrometers, both to evaluate the resolution (or at least a first guess) and to minimize the uncertainty through a proper choice of the geometry and the coefficient α, β and γ.

Consider the AdvSND detector in Figure 1. The first part of the spectrometer design consists in defining the coefficients α, β and γ, the magnetic field B, and the geometry of the scheme in Figure 2, namely x_{12}, x_{23} and x_{34}. A second part of the design, out of the scope of this work, will define also the geometry of the magnet section, i.e. the coil thickness, the yoke thickness, the current density, etc. [2, 3].
In the following, we assume that the relation between momentum resolution $\sigma[\hat{P}]/p$ and the reciprocal momentum resolution $\sigma[\hat{\Pi}]/p^{-1}$ is strictly monotonic, as visible in Figure 4. Hence, the minimization of the momentum uncertainty is achieved by minimizing the uncertainty of the reciprocal, whose expression is provided in (14).
Concerning the spectrometer geometry, the calorimeter length x_{12} and the total length $x_{12}+x_{23}+x_{34}$ are fixed, hence the optimization variables are the ratio between x_{23} and x_{34}, the magnetic fields B_1 and B_2 and the coefficients set (α, β, γ). We assume the magnetic field $B_1 = B_2 = 1.5$ T, as this value is rather affordable for iron core magnets and, due to the iron saturation, it stabilizes $\Delta B/B$.
Due to the constraint (8), there is only one degree of freedom for the choice of α, β and γ, as rescaling all the coefficients gives the same momentum estimator

$$\hat{P} = \frac{q}{2} \frac{\mathcal{B}(\alpha, \gamma)}{\alpha\ \overline{S}_4 + (\beta - \alpha)\ \overline{S}_3 + (\gamma - \beta)\ \overline{S}_2 - \gamma\ \overline{S}_0} \tag{26}$$

A parametrization which includes all the possible choices of coefficients is

$$\alpha = \sin\varphi\ , \qquad \beta = -\frac{\alpha x_{34} + \gamma x_{02}}{x_{23}}\ , \qquad \gamma = \cos\varphi \tag{27}$$

The predicted resolution for the momentum reciprocal is represented in Figure 6 as function of the length of the second magnet, for a given momentum $p = 850$ GeV/c and total length $x_{14} = 488$ cm. In the figure, the solid lines represent the resolution when the particle originates at the end of the target ($x_{01} = 0$ cm) while the dashed lines represent the resolution when the particle originates at the front of the target ($x_{01} = 100$ cm)
Among all the possible choices of coefficients, four of them are shown in Figure 6:

- the red line is the optimal coefficients that optimize the resolution at $p = 850$ GeV/c
- the blue line is a generalization of the standard approach ($\beta = 0$)
- the green line is the resolution achievable without the second magnet ($\alpha = 0$)
- the violet line is the resolution achievable without magnetizing the calorimeter ($\gamma = 0$).

Note that $\alpha = 0$ and $\gamma = 0$ only require three tracking stations, the $\beta = 0$ is considered a generalization of the standard approach[1, 4, 5] because in the case $x_{01} = 0$ cm, it gives

$$\hat{P} = \frac{q}{2}\ \frac{B(f\, x_{12} + x_{34})}{\dfrac{\overline{S}_4 - \overline{S}_3}{x_{34}} - \dfrac{\overline{S}_2 - \overline{S}_1}{x_{12}}} = q\frac{B(f\, x_{12} + x_{34})}{\Delta\theta} \tag{28}$$

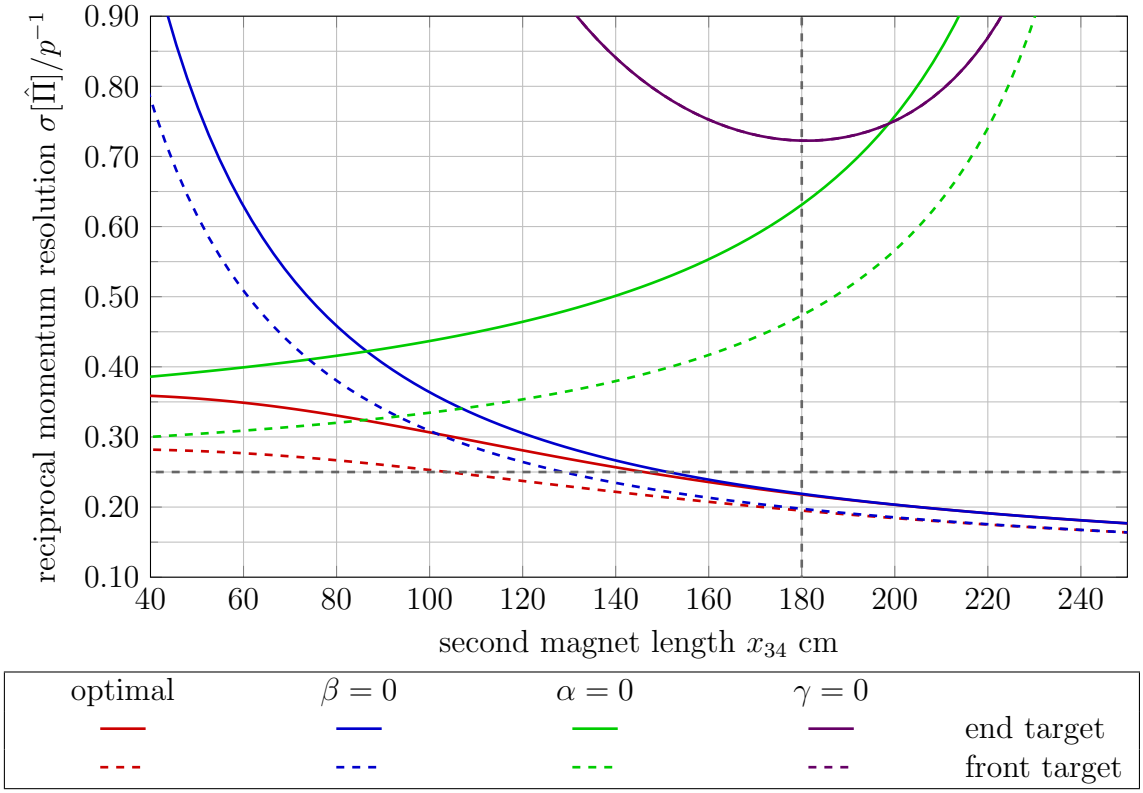

Figure 6: Resolution of the momentum reciprocal as function of the second magnet length, for momentum $p = 850$ GeV/c and total length $x_{14} = 488$. Different colors are used for different sets of coefficients (α, β, γ) as described in the legend. Solid lines are used for the case $x_{01} = 0$ cm (particle generated at the end of the target), dashed lines are used for the case $x_{01} = 100$ cm (particle generated at the front of the target).

where $\Delta\theta$ is the angle variation of the particle, f is the filling factor of the calorimeter (see Appendix) so that fx_{12} is the length of the path in the calorimeter field, and the formula (28) is the one usually applied in the literature.
Due to safety reasons, the spectrometer of AdvSND needs at least x_{23} =90 cm of gap between magnets to not obstruct the tunnel, the maximum size x_{34} for the magnet is hence 180 cm (indicated with the vertical dashed grey line in Figure 6). The maximum length also gives the best resolution, hence the magnet design will be the one reported in the table 1.

x_{12}	x_{23}	x_{34}	B_1	B_2
218 cm	90 cm	180 cm	1.5 T	1.5 T

Table 1: List of parameters of the design.

The same analysis can be done using a fixed x_{23} and variable x_{34}, changing the total

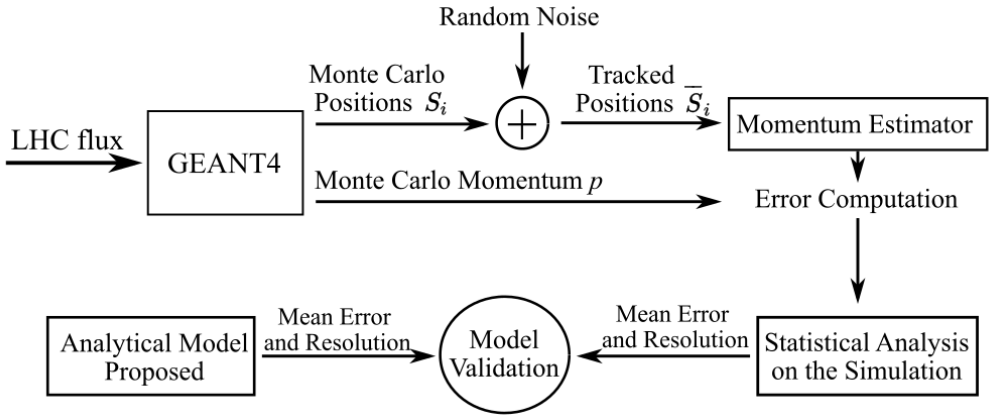

Figure 7: Schematic representation of the numeric computation of the error.

length of the spectrometer. The results of the analysis are again represented by the curves in Figure 6, since the resolution does not depend on x_{23} when $\beta = 0$.

4 GEANT4 cross Validation

In this section the accuracy of the proposed analytical model is tested. The validation is performed through comparison with Montecarlo simulation executed with GEANT4 [6]. A large number of muon neutrino charged current interactions are simulated in the target region and both momentum and positions at each tracking station of the outgoing muons are saved and used for the statistical analysis. The momentum reconstructed from the particle position is compared with the Monte Carlo true momentum of the particle to compute the average error and the detector resolution. Numerical results are compared with the values predicted by the analytical model. The momentum and position distribution of the generated muon is computed by GEANT4 considering the flux of neutrinos coming from the LHC in the angular region where the detector is placed, i.e. $7.2 < \eta < 8.4$. The comparison procedure is schematically represented Figure 7.

4.1 Validation without Scattering - Air Core Magnet

Consider an air core spectrometer based on the bending angle measurement[1, 4], represented in Figure 8. Let the length of the magnet be $\ell_{\mathrm{m}} = 2$ m, the lever arms (before and after the magnet) be $\ell = 1$ m, and the trackers resolution is $\varepsilon = 100$ μm.

Using the notation and procedures presented in the previous sections, with $x_{12} = x_{34} = \ell$ and $x_{23} = \ell_{\mathrm{m}}$, the momentum reciprocal estimator is

$$\hat{\Pi} = \frac{qB\ell_m}{2} \frac{\alpha\ \overline{S}_4 + (\beta - \alpha)\ \overline{S}_3 + (\gamma - \beta)\ \overline{S}_2 - \gamma\ \overline{S}_0}{2\alpha\ell + \beta\ell_{\mathrm{m}}} \tag{29}$$

with the constraint $\ell\alpha + \ell_{\mathrm{m}}\beta + \ell\gamma = 0$. It is straightforward to prove that the minimum standard deviation is obtained for $\alpha = 1$, $\beta = 0$ and $\gamma = -1$, so that the

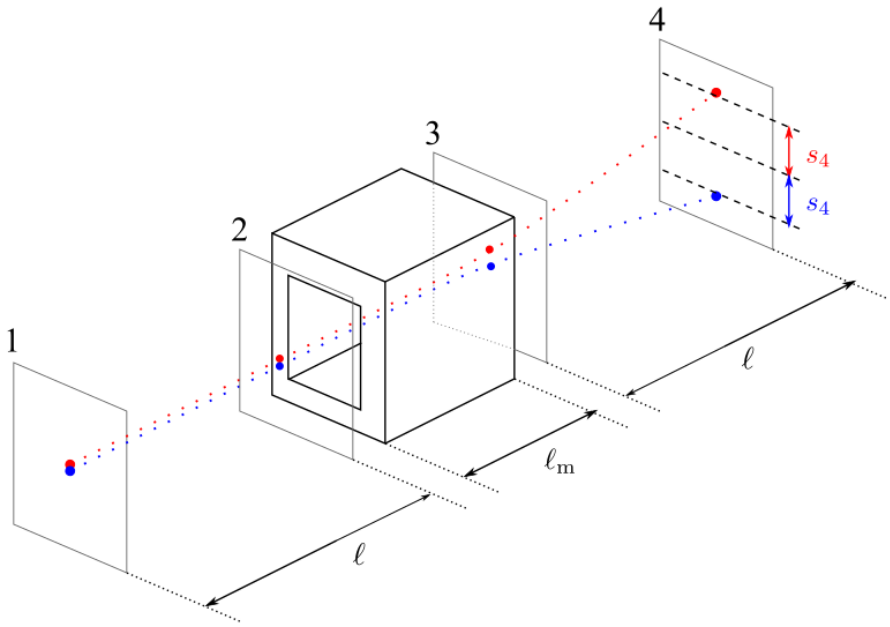

Figure 8: Schematic representation of the configuration for the bending angle measurement with air core magnet.

momentum estimator is

$$\hat{P} = \frac{qB\,\ell\,\ell_{\mathrm{m}}}{\overline{S}_4 - \overline{S}_3 - \overline{S}_2 + \overline{S}_1} \tag{30}$$

Remarkably, the resolution computed within the first order approximation is the well known formula usually applied for the spectrometer design[1, 4]

$$\left.\frac{\Delta p}{p}\right|_{\text{first order}} = \frac{2\varepsilon p}{qB\,\ell\,\ell_{\mathrm{m}}} \tag{31}$$

For the validation $489 \cdot 10^3$ events are simulated with GEANT4, gaussian noise is added to the trackers measurement with zero mean and standard deviation ε and the threshold momentum was set to 3 TeV/c. The simulated events are divided in classes depending on the momentum of the particle generated in the simulation and, we compute for each momentum class the momentum resolution and the average relative error, namely

$$err = \mathbb{E}\left[\frac{\hat{P} - p}{p}\right] = \mathbb{E}\left[\frac{\hat{P}}{p}\right] - 1 = \frac{\mathbb{E}\left[\hat{P}\right] - p}{p} \tag{32}$$

The comparison between simulation and analytics is shown in Figure 9 and Figure 10 for the standard deviation and the mean relative error, respectively, as function of the particle momentum p.
As expected, the first order approximation is accurate only for resolution up to $\Delta p/p \approx 0.15$, and it underestimate the uncertainty for higher values until the cutoff effect become become prevalent.

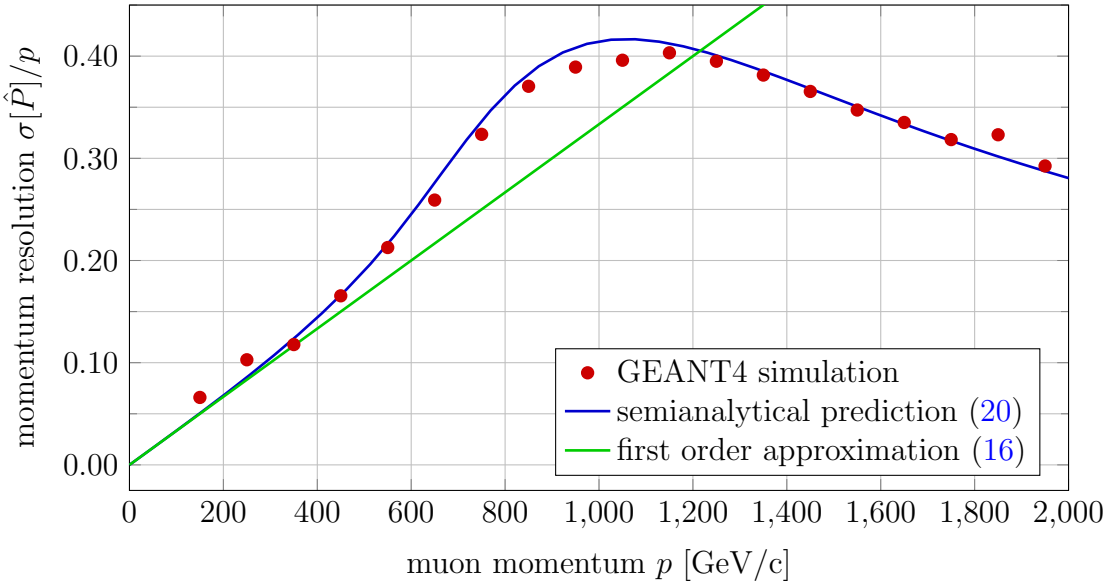

Figure 9: Momentum resolution as function of the particle momentum. Dots in blue are the given blue the numerical simulations, solid lines are given by analytics.

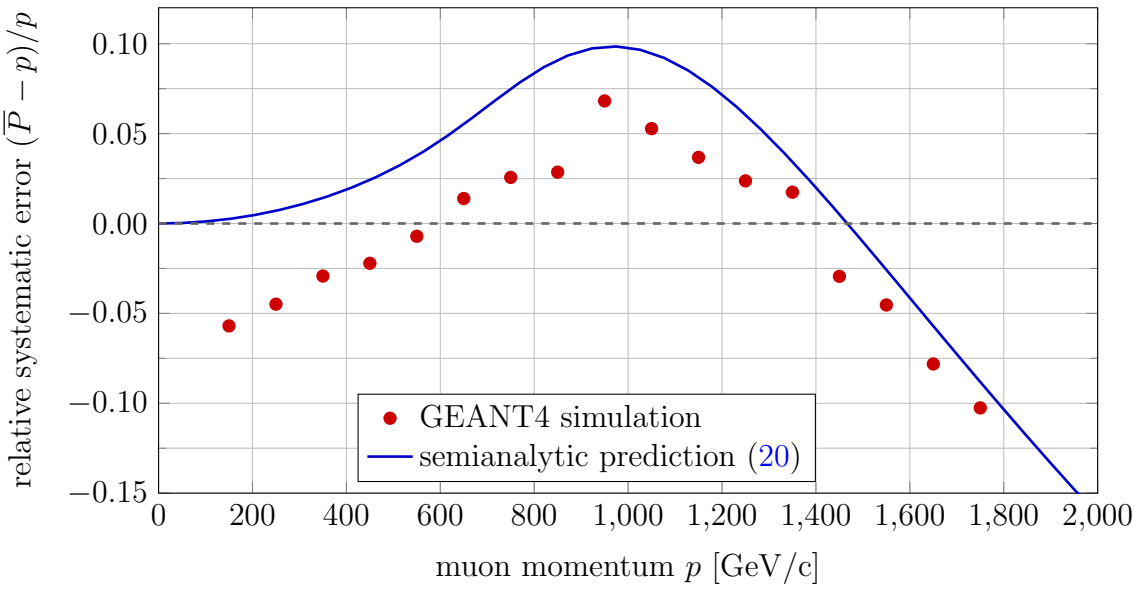

Figure 10: Average relative error as function of the particle momentum. Dots in blue are the given blue the numerical simulations, solid lines are given by analytics.

The relative error plot can be divided in three regions:

- At low momentum, the momentum loss due to scattering in the iron is dominant and the average measurement error is negative
- At intermediate momentum, the distortion of the estimator is dominant and the average measurement error is positive

- At high momentum, the cut-off effect is dominant and the average measurement error is negative

4.2 Validation with Scattering - AdvSND FAR Detector

In this section, we consider the design of the AdvSND FAR detector proposed in Table 1. Since the optimal set of coefficients (α, β, γ) depends on p, which is not known, for the sake of simplicity we use the set with $\beta = 0$ which performs well for the geometry chosen (see Figure 6). The momentum estimator is then

$$\hat{P} = \frac{q}{2} \frac{x_{02}x_{34}[x_{34}B_2' + (x_{12} + 2x_{01})B_1^*]}{x_{02}\overline{S}_4 - x_{02}\overline{S}_3 - x_{34}\overline{S}_2 + x_{34}\overline{S}_0} \tag{33}$$

where the field B_2' include a multiplicative factor (see the Appendix) to take into account the space between tracking station and magnet.
The field is assumed to be piecewise constant in the GEANT4 model. A sample of $59{\cdot}10^3$ events is simulated and a gaussian noise is added to the trackers measurement. The cut-off threshold is set to $p_{\max} = 2000$ GeV/c, reducing the valid sample size to $58 \cdot 10^3$. The comparison between semi-analytical model and simulation is presented in Figure 11.
The statistics on the simulated events is in good agreement with the analytical prediction, the discrepancy of the resolution for high values of the momentum is mostly due to the fact that only a small number of particles have momentum over 1400 GeV/c (less than 10^3), hence the statistical sample size is too small to yield an accurate statistics.

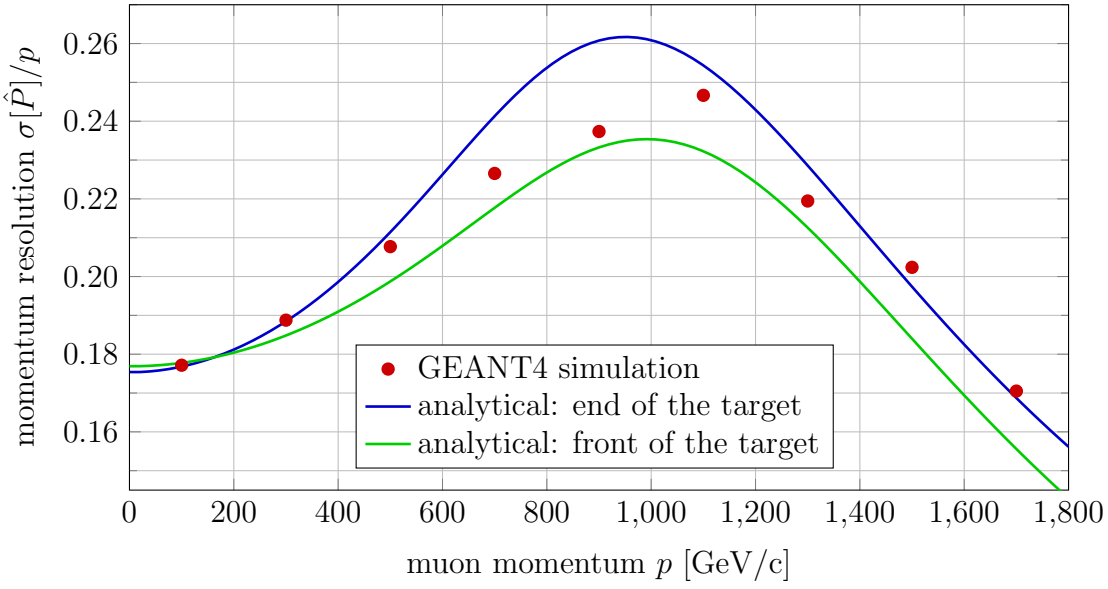

Figure 11: Momentum resolution for the configuration in Figure 1 and data in Table 1 as function of the particle momentum. Dots are the numerical results, lines are the semi-analytic results for particles generated at the target front or the target end (see the legend).

5 Conclusion

The work proposes a set of analytical and semi-analytical tools for the geometrical design of a spectrometer for high energy physics experiments.
The proposed methods allow a simple analysis of the spectrometer performance, even for non usual configurations in terms of geometry and magnetic field. Implementing the model's equation in a code, a fast optimization procedure can be executed. Alternatively, the model can be coupled with analytical models for the engineering design to perform a coupled design with a very low computational cost.
In this work, the model is applied to determine the geometry of the AvdSND FAR magnet achieving the best momentum resolution compatible with external constraints due to the available space and safety.
The results are validated via simulation with Monte Carlo simulation executed with GEANT4. Comparison shows a very good agreement between analytics and numerical for the in the range 0-1400 GeV/c for the momentum resolution, validating the semi-analytical model.

A Scattering Evaluation

The scattering contribution is based on the assumption that scattering angles behave like a Wiener process[7] which is compatible with the small angle approximation. According to the Molliere theory[5, 8], the variance of the scattering angle θ_σ of a particle with momentum p, travelling in the matter for a distance X is

$$\sigma^2[\Theta_\sigma] = \frac{P_0^2}{p^2}\frac{X}{X_0}. \tag{34}$$

where P_0 is a constant, X_0 is the radiation length[5] of the medium. In this document we use $P_0 = 15$ MeV/c, while the radiation lengths for iron and tungsten are $X_{\text{Fe}} = 1.76$ cm and $X_{\text{W}} = 0.35$ cm, respectively.
The displacement due to scattering is obtained by integrating the angle along the path length

$$\begin{aligned}\sigma^2[S_\sigma] &= \mathbb{E}\left[\left(\int_0^X \Theta_\sigma(x)\,\mathrm{d}x\right)^2\right] = \iint \mathbb{E}[\Theta_\sigma(x)\Theta_\sigma(y)]\,\mathrm{d}x\,\mathrm{d}y \\ &= \frac{P_0^2}{p^2}\frac{1}{X_{\text{Fe}}}\iint \min(x,y)\,\mathrm{d}x\,\mathrm{d}y = \frac{P_0^2}{p^2}\frac{2}{X_0}\int_0^X \mathrm{d}x\int_0^x y\,\mathrm{d}y \\ &= \frac{P_0^2}{p^2}\frac{1}{X_0}\int_0^X x^2\mathrm{d}x = \frac{P_0^2}{p^2}\frac{X}{X_0}\frac{X^2}{3}\end{aligned} \tag{35}$$

Note that the scattering angle and displacement are correlated, the variance of a generic combination of them is given by

$$\begin{aligned}\sigma^2[S_\sigma + Y\Theta_\sigma] &= \mathbb{E}\left[\left(\int_0^X \Theta_\sigma(x)\,\mathrm{d}x + Y\Theta_\sigma(X)\right)^2\right] \\ &= \iint \mathbb{E}[\Theta_\sigma(x)\Theta_\sigma(y)]\,\mathrm{d}x\,\mathrm{d}y + Y^2\mathbb{E}[\Theta_\sigma^2(X)] + 2Y\int \mathbb{E}[\Theta_\sigma(x)\Theta_\sigma(X)]\,\mathrm{d}x \\ &= \frac{P_0^2}{p^2}\frac{X}{X_0}\frac{X^2}{3} + \frac{P_0^2}{p^2}\frac{X}{X_0}Y^2 + 2\frac{P_0^2}{p^2}\frac{Y}{X_0}\int_0^X x\,\mathrm{d}x \\ &= \frac{P_0^2}{p^2}\frac{X}{X_0}\left(\frac{X^2}{3} + Y^2 + XY\right)\end{aligned} \tag{36}$$

Finally, applying (35) and (36) to the terms in (11) we obtain (after some algebra)

$$\sigma^2[S_{\sigma 34}] = \frac{P_0^2}{p^2}\frac{x_{34}}{X_{\text{Fe}}}\frac{x_{34}^2}{3} \tag{37}$$

$$\sigma^2[S_{\sigma 12} - x_{02}\Theta_{\sigma 12}] = \frac{P_0^2}{p^2}\frac{x_{12}}{X_{\text{Fe}}^*}\left(\frac{x_{12}^2}{3} + x_{01}x_{02}\right) \tag{38}$$

$$\sigma^2[S_{\sigma 01} - x_{01}\Theta_{\sigma 01}] = \frac{P_0^2}{p^2}\frac{x_{01}}{X_{\text{W}}}\frac{x_{01}^2}{3} \tag{39}$$

where the corrected radiation length $X_{\text{Fe}}^* = X_{\text{Fe}}(\Delta x/\Delta x_{\text{Fe}})$ is presented in the next section.

B Field and Scattering in the Calorimeter

The calorimeter is composed by several iron slabs separated by small air gap where sensors are located. In this section the effects of scattering in the calorimeter are analyzed. Let S_i and Θ_i the displacement and the angle of the particle at the i-th interface, we have

$$\begin{cases} S_{i+1} - S_i = \theta_i \Delta x_i + \frac{1}{2}\frac{qB_i}{p}\Delta x_i^2 + S_{\sigma i} \\ \Theta_{i+1} - \Theta_i = \frac{qB_i}{p}\Delta x_i + \Theta_{\sigma i} \end{cases} \tag{40}$$

where B_i is the magnetic field, Δx is the distance between interfaces, S_σ and Θ_σ are the displacement and the angle deviation due to scattering, and the subscript i is used to denote these quantities in the region between the i-th and the $i+1$-th interfaces.
In a calorimeter, all iron slabs and air gaps have thickness Δx_{Fe} and Δx_{air} respectively. Moreover, we can assume that the scattering effects and the magnetic field in the air gaps are negligible. Combining the effects of an iron slab and an air gap, we have

$$\begin{cases} S_{i+2} - S_i = \theta_i(\Delta x_{\text{Fe}} + \Delta x_{\text{air}}) + \frac{qB_{\text{Fe}}}{p}\left(\frac{1}{2}\Delta x_{\text{Fe}} + \Delta x_{\text{air}}\right)\Delta x_{\text{Fe}} + S_{\sigma i} + \Theta_{\sigma i}\Delta x_{\text{air}} \\ \Theta_{i+2} - \Theta_i = \frac{qB_{\text{Fe}}}{p}\Delta x_{\text{Fe}} + \Theta_{\sigma i} \end{cases} \tag{41}$$

Finally, we consider N layer of iron slab - air gap to have the total deviation of the particle in the calorimeter. After some algebra, it yields

$$\begin{cases} S = & S_0 + \Theta_0 N(\Delta x_{\text{Fe}} + \Delta x_{\text{air}}) \\ & \quad + \frac{qB_{\text{Fe}}}{2p}\left[N(N-1)(\Delta x_{\text{Fe}} + \Delta x_{\text{air}}) + N\left(\Delta x_{\text{Fe}} + 2\Delta x_{\text{air}}\right)\right]\Delta x_{\text{Fe}} \\ & \quad + \sum_{i=0}^{N} S_{\sigma i} + \Theta_{\sigma i}[(N-i)\Delta x_{\text{Fe}} + (N-i+1)\Delta x_{\text{air}}] \\ \Theta = & \Theta_0 + \frac{qB_{\text{Fe}}}{p} N\Delta x_{\text{Fe}} + \sum_{i=0}^{N}\Theta_{\sigma i} \end{cases} \tag{42}$$

where the i subscript now denotes the scattering in the i-th slab of iron.
From the last equation, the mean value and variance of the angle Θ are

$$\mathbb{E}[\Theta] = \Theta_0 + \frac{qB'_{\text{Fe}}}{p} fX \ , \qquad \sigma^2[\Theta] = \frac{P_0^2}{p^2}\frac{fX}{X_{\text{Fe}}} = \frac{P_0^2}{p^2}\frac{X}{X^*_{\text{Fe}}} \tag{43}$$

where $X = N(\Delta x_{\text{Fe}} + \Delta x_{\text{air}})$ is the total length of the spectrometer, $f = \frac{\Delta x_{\text{Fe}}}{\Delta x_{\text{Fe}} + \Delta x_{\text{air}}}$ is the filling factor of the calorimeter, $X^*_{\text{Fe}} = X_{\text{Fe}}/f$ is an equivalent radiation length, and $B'_{\text{Fe}} = B_{\text{Fe}} f$ is an equivalent magnetic field.
The expressions of the mean value and variance of the displacement S are relatively complex, however a simple expression is obtained in the limit of high number of

slabs. In the limit for high N it gives

$$S \xrightarrow{N} S_0 + \Theta_0 X + \frac{qB'_{\text{Fe}}}{2p} X^2 + \sum_{i=0}^{N} S_{\sigma i} + \Theta_{\sigma i}(N-i)\Delta x \tag{44}$$

where $\Delta x = (\Delta x_{\text{Fe}} + \Delta x_{\text{air}})$.
Finally, changing the summation index the variance of S gives in the limit of high N

$$\sigma^2[S] \approx \frac{1}{3}\frac{P_0^2}{p^2}\frac{\Delta x_{\text{Fe}}}{X_{\text{Fe}}}\sum_{i=0}^{N}\left(\Delta x_{\text{Fe}}^2 + 3i^2\Delta x^2 + 3i\Delta x\Delta x_{\text{Fe}}\right) \xrightarrow{N} \frac{1}{3}\frac{P_0^2}{p^2}\frac{\Delta x_{\text{Fe}}}{X_{\text{Fe}}}N^3\Delta x^2 = \frac{1}{3}\frac{P_0^2}{p^2}\frac{X}{X^*_{\text{Fe}}}X^2 \tag{45}$$

C Tracker Space Correction

In this section, we take into account the distance between tracking stations and magnet. The equation of motion are

$$\begin{cases} \Theta_1 = \Theta_0 \\ S_1 = S_0 + \Theta_0 x_a \end{cases} \qquad \begin{cases} \Theta_2 = \Theta_1 + \dfrac{qB}{p}x_f + \Theta_\sigma \\ S_2 = S_1 + \Theta_1 x_f + \dfrac{qB}{2p}x_f^2 + S_\sigma \end{cases} \qquad \begin{cases} \Theta_3 = \Theta_2 \\ S_3 = S_2 + \Theta_2 x_a \end{cases} \tag{46}$$

where x_a is the distance between tracking station and magnet.
Replacing S_1 and S_2 in the expression of S_3 it yields

$$\begin{cases} \Theta_3 = \Theta_0 + \dfrac{qB}{p}x_{\text{Fe}} + \Theta_\sigma \\ S_3 = S_0 + \Theta_0 X + \dfrac{qB}{2p}x_{\text{Fe}}X + S_\sigma + x_a\Theta_\sigma \end{cases} \implies \begin{cases} \Theta_3 = \Theta_0 + \dfrac{qB'}{p}X + \Theta_\sigma \\ S_3 = S_0 + \Theta_0 X + \dfrac{qB'}{2p}X^2 + S'_\sigma \end{cases} \tag{47}$$

where $X = x_f + 2x_a$ is the total distance between trackers, $B' = B\ (x_{\text{Fe}}/X)$ is an equivalent magnetic field, and $S'_\sigma = S_\sigma + x_a\Theta_\sigma$ is an equivalent scattering and its variance can be computed with (36).

D Variable Magnetic Field

In this section, we consider a non piece-wise constant magnetic field in the spectrometer. Consider a spectrometer with 4 tracking station and, to keep the math simple, neglect the particle scattering. The effects of scattering is straightforward, but not necessary for the scope of this section. The equations of motion for the displacement

are

$$\begin{aligned} S_4 - S_3 &= \Theta_3 x_{34} + \frac{q}{p} \int_{x_{13}}^{x_{14}} \mathrm{d}x \int_{x_{13}}^{x} B(y)\ \mathrm{d}y \\ S_3 - S_2 &= \Theta_2 x_{23} + \frac{q}{p} \int_{x_{12}}^{x_{13}} \mathrm{d}x \int_{x_{12}}^{x} B(y)\ \mathrm{d}y \\ S_2 - S_1 &= \Theta_1 x_{12} + \frac{q}{p} \int_{0}^{x_{12}} \mathrm{d}x \int_{0}^{x} B(y)\ \mathrm{d}y \end{aligned} \tag{48}$$

where $x_{13} = x_{12} + x_{23}$ and $x_{14} = x_{13} + x_{34}$, and for the angle they are

$$\begin{aligned} \Theta_3 &= \Theta_2 + \frac{q}{p} \int_{x_{12}}^{x_{13}} B(y)\ \mathrm{d}y \\ \Theta_2 &= \Theta_1 + \frac{q}{p} \int_{0}^{x_{12}} B(y)\ \mathrm{d}y \end{aligned} \tag{49}$$

The momentum reciprocal is then given by

$$\frac{1}{p} = \frac{1}{q} \frac{\alpha S_4 + (\beta - \alpha) S_3 + (\gamma - \beta) S_2 - \gamma S_1}{\alpha \mathcal{B}_i(x_{13}, x_{14}) + \beta \mathcal{B}_i(x_{12}, x_{13}) + \gamma \mathcal{B}_i(0, x_{12})} \tag{50}$$

where

$$\mathcal{B}_i(x_a, x_b) = (x_b - x_a) \int_0^{x_a} B(x)\ \mathrm{d}x + \int_{x_a}^{x_b} \mathrm{d}x \int_{x_a}^{x} B(y) \mathrm{d}y \tag{51}$$

and the constraint $\alpha x_{34} + \beta x_{23} + \gamma x_{12} = 0$ is imposed.
In the general case, (50) must studied numerically, once the magnetic field is known, either from measures or 3D FEM simulation, or possibly in a loop with the 3D simulation.
As an example, consider again the configuration in Figure 8. Due to the symmetry of the geometry ($x_{12} = x_{34}$), we can assume the field is symmetric, namely $B(x_c + x) = B(x_c - x)$, where $x_c = x_{12} + x_{23}/2$. Using $\beta = 0$ and $\alpha = -\gamma$, the momentum reciprocal is

$$\frac{1}{p} = \frac{1}{q} \frac{S_4 - S_3 - S_2 + S_1}{\displaystyle\int_{x_{13}}^{x_{14}} \mathrm{d}x \int_{x_{13}}^{x} B(y)\ \mathrm{d}y - \int_{0}^{x_{12}} \mathrm{d}x \int_{0}^{x} B(y)\ \mathrm{d}y + x_{34} \int_{0}^{x_{13}} B(y)\ \mathrm{d}y} \tag{52}$$

After some algebra, using the symmetry condition, the two double integral are recast as

$$\begin{aligned} &\int_{0}^{x_{12}} \mathrm{d}x \int_{x}^{x_{12}} B(y)\ \mathrm{d}y - \int_{0}^{x_{12}} \mathrm{d}x \int_{0}^{x} B(y)\ \mathrm{d}y = \\ &\int_{0}^{x_{12}} \int_{0}^{x_{12}} \mathrm{sgn}(y - x) B(y)\ \mathrm{d}x \mathrm{d}y = \int_{0}^{x_{12}} (2x - x_{12}) B(x)\ \mathrm{d}x \end{aligned} \tag{53}$$

Assuming the strongest field is in the magnet region, the denominator of (52) is positive and the term (53) due to the field outside the magnet gives a positive contribution. The field in the regions before the second tracker and after the third tracker gives a smaller contribution to the bending power, nonetheless their effect improves the resolution (althought it is very small) and introduces a systematic error if not taken into account.

References

[1] J. L. Feng et al., *The Forward Physics Facility at the High-Luminosity LHC*, *Journal of Physics G: Nuclear and Particle Physics* **50** (Jan, 2023) 030501.

[2] C. Ahdida et al., *The magnet of the scattering and neutrino detector for the ship experiment at cern*, *Journal of Instrumentation* **15** (jan, 2020) P01027.

[3] D. Centanni, D. Davino, M. de Magistris, R. Fresa, V. P. Loschiavo, A. Quercia, and V. Scalera, *Power-efficient design of large-aperture magnets for high-energy physics*, *Sustainability* **15** (2023), no. 14.

[4] R. M. Abraham et al., *Tau neutrinos in the next decade: from GeV to EeV*, *Journal of Physics G: Nuclear and Particle Physics* **49** (2022), no. 11.

[5] C. Grupen and I. Buvat, *Handbook of Particle Detection and Imaging*. Springer, 1st ed., 2012.

[6] **GEANT4** Collaboration, *Geant4—A simulation toolkit*, *Nuclear Instruments and Methods in Physics Research Section A: Accelerators, Spectrometers, Detectors and Associated Equipment* **506** (2003) 250–303.

[7] C. Gardiner, *Stochastic Methods: A Handbook for the Natural and Social Sciences*. Springer, 4th ed., 2009.

[8] V. Highland, *Some Practical Remarks on Multiple Scattering*, *Nuclear Instruments and Methods* **129** (1975) 497–499.